JACS
JOURNAL OF THE AMERICAN CHEMICAL SOCIETY
Article
pubs.acs.org/JACS

Large-Scale Production of Graphene Nanoribbons from Electrospun Polymers

Nan Liu,[†] Kwanpyo Kim,[†,⊥] Po-Chun Hsu,[‡] Anatoliy N. Sokolov,[†,▽] Fung Ling Yap,[†,#] Hongtao Yuan,[§,∥] Yanwu Xie,[§,∥] Hao Yan,[‡,∥] Yi Cui,[‡,∥] Harold Y. Hwang,[§,∥] and Zhenan Bao*[,†]

[†]Department of Chemical Engineering, [‡]Department of Materials Science and Engineering, and [§]Geballe Laboratory for Advanced Materials, Department of Applied Physics, Stanford University, Stanford, California 94305, United States

[∥]Stanford Institute for Materials and Energy Sciences, SLAC National Accelerator Laboratory, Menlo Park, California 94025, United States

[⊥]Department of Physics, Ulsan National Institute of Science and Technology (UNIST), Ulsan 689-798, Korea

[#]Institute of Materials Research and Engineering (IMRE), Agency for Science, Technology and Research (A*STAR), 3 Research Link, 117602 Singapore

Supporting Information

ABSTRACT: Graphene nanoribbons (GNRs) are promising building blocks for high-performance electronics due to their high electron mobility and dimensionality-induced bandgap. Despite many past efforts, direct synthesis of GNRs with controlled dimensions and scalability remains challenging. Here we report the scalable synthesis of GNRs using electrospun polymer nanofiber templates. Palladium-incorporated poly(4-vinylphenol) nanofibers were prepared by electrospinning with controlled diameter and orientation. Highly graphitized GNRs as narrow as 10 nm were then synthesized from these templates by chemical vapor deposition. A transport gap can be observed in 30 nm-wide GNRs, enabling them to function as field-effect transistors at room temperature. Our results represent the first success on the scalable synthesis of highly graphitized GNRs from polymer templates. Furthermore, the generality of this method allows various polymers to be explored, which will lead to understanding of growth mechanism and rational control over crystallinity, feature size and bandgap to enable a new pathway for graphene electronics.

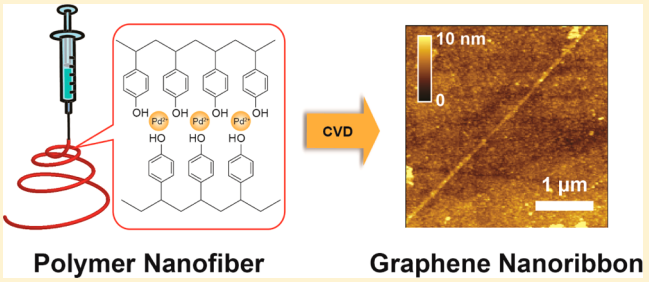

INTRODUCTION

Graphene has attracted broad interest due to its superior electronic properties, such as high charge carrier mobility and conductivity. These properties make it an exciting material in radio frequency (RF) electronics, flexible touch screen displays, high-performance sensors, supercapacitors and batteries.[1−8] However, graphene is a zero-bandgap semimetal,[9] which limits its application as channel material for field-effect transistors (FETs). To make graphene truly usable in digital electronics, it is thus crucial to introduce a bandgap in this material. Constraining two-dimensional (2D) graphene into one-dimensional (1D) graphene nanoribbon (GNR) can be a very effective way to create a bandgap.[10] Several efforts have been made to create GNRs. For example, GNRs can be etched from 2D graphene sheets using both self-assembled and lithographically defined masks.[11,12] These etching methods, however, usually introduce rough edges and defects into the GNRs, which undermines their electrical performances. High-quality and narrow GNRs can be produced by unzipping carbon nanotubes (CNTs),[13−15] but the low throughput of this approach severely limits its scalability. On the other hand, GNRs can be directly synthesized on 1D templates. For example, GNRs with 40 nm width can be epitaxially grown on the step edges of SiC,[16] although the lack of bandgap in these GNRs has hindered their incorporation as FETs in digital electronics.

Chemical vapor deposition (CVD) is a powerful tool for large-scale production of graphitic structures.[17,18] In analogy to the CVD growth of 2D graphene on metal sheets, GNRs can be directly grown from 1D metal catalysts such as nickel edges and nanobars.[19,20] However, the high surface mobility of the metal catalysts during the high-temperature CVD process can lead to metal agglomeration on the growth substrate, resulting in short discontinuous GNRs. On the other hand, metal catalysts in the form of cations can be chemically anchored on 1D nanostructures such as DNA chains to prevent their agglomeration. Indeed CVD on such metal-incorporated 1D templates can lead to the growth of GNRs,[21] although the abundant heteroatoms (nitrogen and phosphor) in DNA

Received: September 28, 2014
Published: November 19, 2014

   dx.doi.org/10.1021/ja509871n | J. Am. Chem. Soc. 2014, 136, 17284−17291

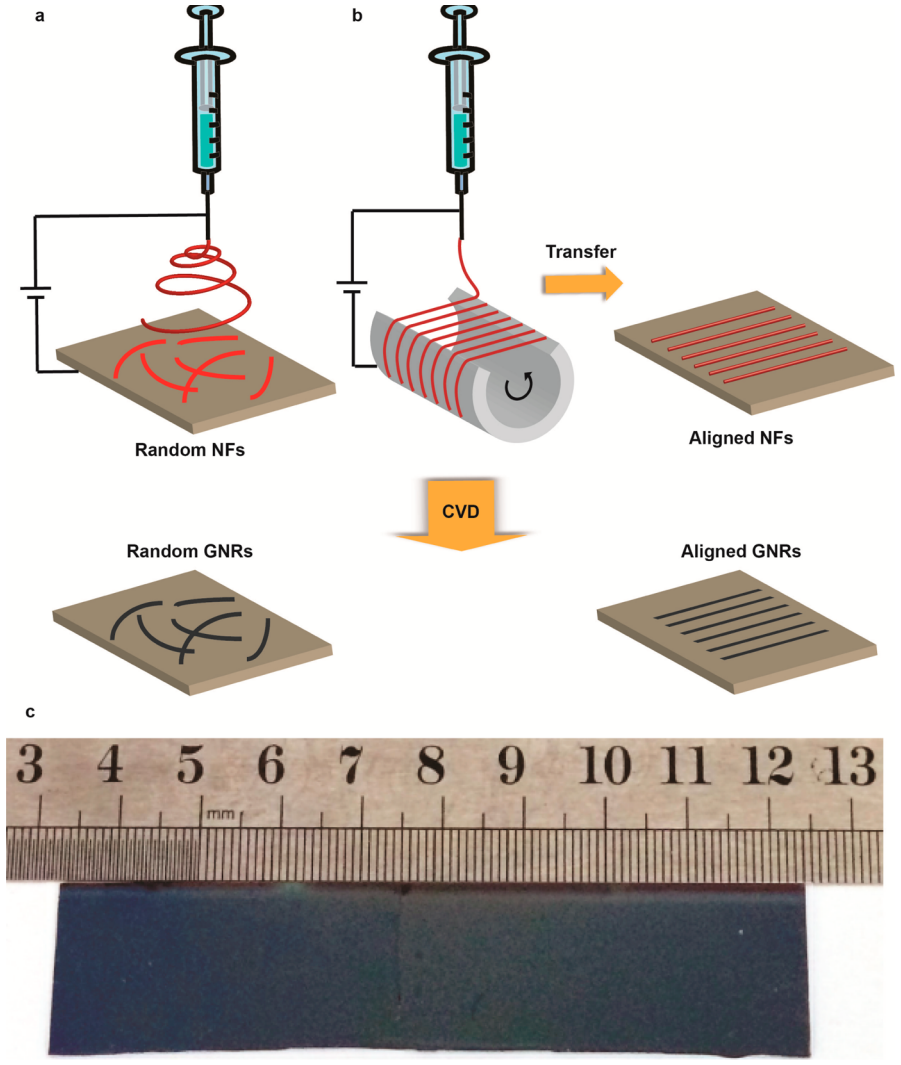

Figure 1. Schematic process of CVD synthesis of GNRs from electrospun polymer templates. (a) Deposition of random nanofiber networks on the growth substrate. (b) Formation of aligned nanofibers on a metallic rotor with a gap and subsequent transfer onto the growth substrate. (c) Photograph of a Si/SiO_2 wafer with GNRs. A ruler is placed on top for size comparison.

interfere with the formation of highly crystalline graphitic structures, resulting in high ratio of sp^3- to sp^2-carbon as well as relatively low conductivity and carrier mobility in these GNRs. Besides, DNAs are unsuitable for large-scale production of GNRs. To enable the mass production of high-quality GNRs, it is thus crucial to establish a generic method to synthesize GNRs from alternative 1D templates. To this end, electrospinning is a powerful tool to create 1D polymer structures with high scalability. A large variety of polymers with metal-binding functional groups can be electrospun, allowing metal catalysts to be stably incorporated while avoiding excessive amount of heteroatoms. Polymer nanofibers as narrow as 5 nm and much longer length (~ cm scale) can be formed by electrospinning, with dimensions suitable for the growth of GNRs with sub-10 nm width.

In this report, we demonstrate the CVD synthesis of high-quality GNRs from metal-incorporated electrospun polymer nanofibers. First, palladium-incorporated poly-4-vinylphenol (Pd@PVP) nanofibers with uniform and tunable diameters were fabricated by electrospinning. These nanofibers can be aligned on the growth substrate. Methane CVD on these nanofiber templates yielded highly graphitic GNRs with well-controlled widths. Interestingly, we discovered a positive correlation between the width of the GNRs and their resistivity. Resistivity as low as 10^{-6} Ωm can be achieved in GNRs of 50 nm width, which is comparable to that of bulk graphite and GNRs derived by etching methods.[14,22] Furthermore, by decreasing the width of the ribbons to ~30 nm, a transport gap can be opened, enabling these narrow GNRs to function as active elements of FETs, with an on/off ratio of ~14 and field-effect mobility as high as ~28 $cm^2/(V\ s)$ at room temperature. These results represent the highest quality GNRs synthesized from polymer templates. Further advancement can be made through exploration of different electronspun polymers as well as precise size control of the electrospun polymer templates. We believe this generic and scalable method is promising for the large-scale production of high-quality GNRs with rationally controlled bandgap and conductivity, which will enable all-GNRs circuits, and pave a new road for the graphene electronics.

EXPERIMENTAL SECTION

Synthesis of GNRs. The Pd@PVP nanofibers were electrospun from a tetrahydrofuran (THF) solution of PVP, $Pd(OAc)_2$ and

dx.doi.org/10.1021/ja509871n | J. Am. Chem. Soc. 2014, 136, 17284−17291

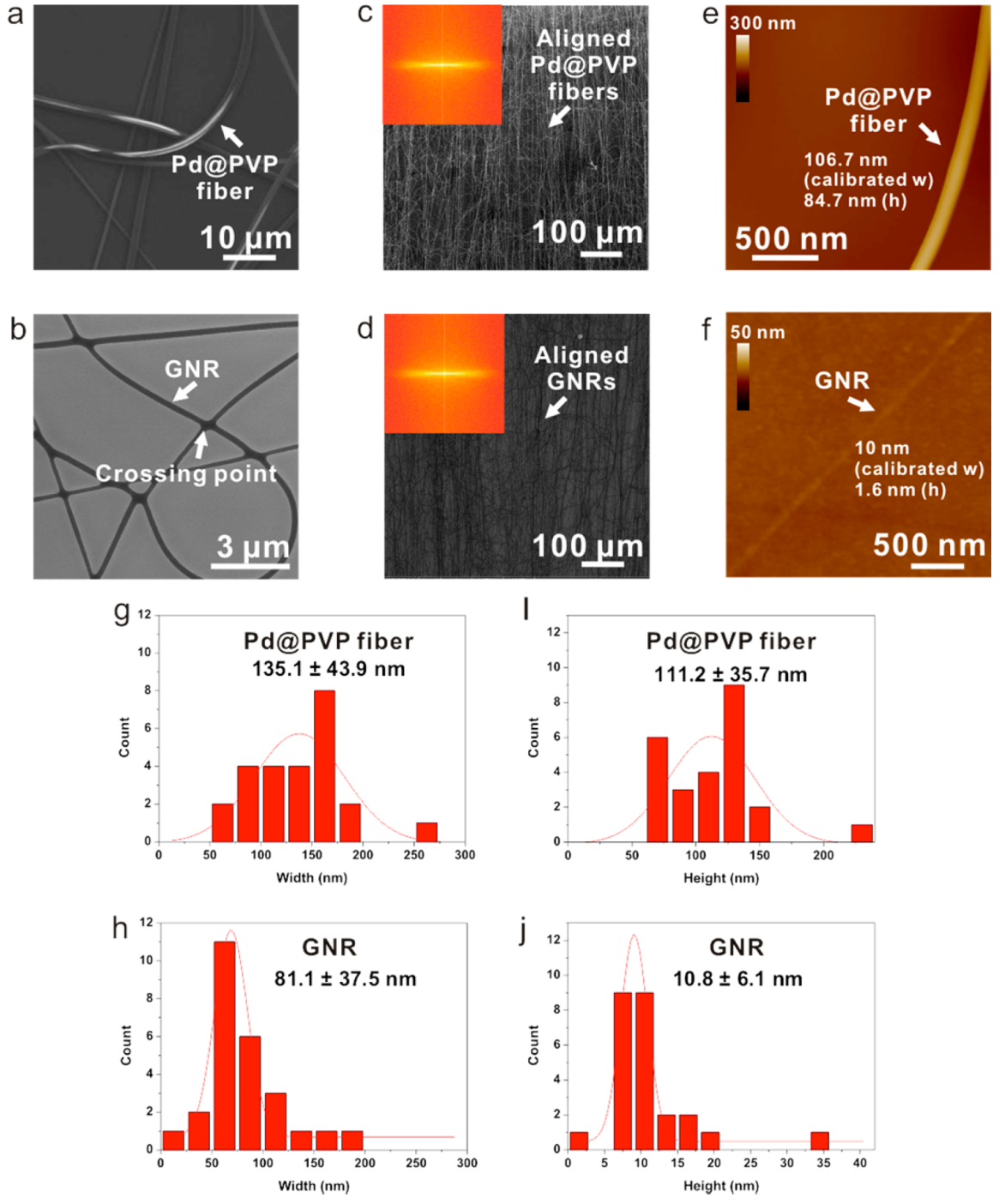

Figure 2. Morphology characterizations of electrospun Pd@PVP fibers and postgrowth GNRs. (a,b) Typical SEM image of electrospun PVP@Pd fibers on SiO_2/Si (a) and GNRs after CVD process (b). (c,d) SEM images of aligned electrospun PVP@Pd fibers on SiO_2/Si (c) and GNRs after CVD process (d). Insets of c, d are their corresponding FFT patterns. (e,f) AFM images of electrospun PVP@Pd fiber on SiO_2/Si (e) and GNR after CVD process (f). (g,h) Width histograms of electrospun Pd@PVP fibers (g) and GNRs (h). (i,j) Height histograms of electrospun Pd@PVP fibers (i) and GNRs (j). All the widths and heights (g–j) were measured by calibrated AFM probes.

myristyl trimethylammonium bromide (MiTMAB). Growth of GNRs was performed in a low-pressure thermal CVD system using methane and hydrogen as the carbon source and carrier gas, respectively. Details of the experimental methods can be found in the Supporting Information.

Characterizations. Dimensions of the GNRs were measured by atomic force microscopy (AFM, Nanoscope-III, Digital Instrument) operated in tapping mode. The convolution effect of the AFM tip was calibrated using a carbon nanotube sample. Raman spectra were taken on a confocal Raman system (WiTec 500) using 532 nm laser excitation. Transmission electron microscopy (TEM) images were taken on a Titan system (FEI) with spherical aberration correction at 80 kV acceleration voltage. Energy-dispersive X-ray spectroscopy (EDS) and electron energy loss spectroscopy (EELS) were carried out on a Tecnai TEM system (FEI) with 200 kV acceleration voltage. X-ray photoelectron spectroscopy (XPS) was carried out with PHI 5000 Versaprobe equipped with monochromatic Al K source. Room-temperature electrical transport was characterized on a probe station with a semiconductor analyzer (Keithley 4200-SCS) and low-

dx.doi.org/10.1021/ja509871n | J. Am. Chem. Soc. 2014, 136, 17284–17291

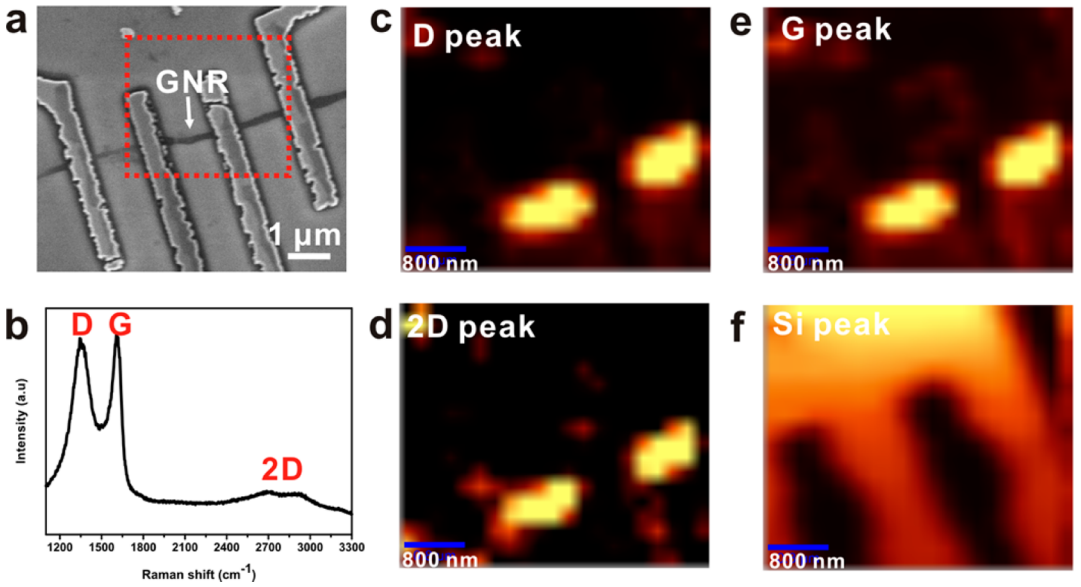

Figure 3. (a) SEM image of a thin GNR with electrodes used for the Raman measurement. (b) Raman spectrum of the GNR taken at the center of the ribbon as shown by the arrowed in (a). (c–f) Integrated Raman intensity mappings of the D peak (1250–1450 cm^{-1}) (c), 2D peak (2450–2750 cm^{-1}) (d), G peak (1500–1700 cm^{-1}) (e) and Si peak (500–550 cm^{-1}) (f) of the region marked by red dotted rectangle in (a).

temperature transport was measured in a Physical Property Measurement System (PPMS, Quantum Design) with a ^{4}He cryostat.

RESULTS AND DISCUSSION

We use electrospinning to achieve 1D polymer templates. Electrospinning is a scalable and versatile technique for the fabrication of polymer nanofibers.[23] A large variety of polymers can be electrospun.[23] Additionally, the width/diameters of the nanofibers can be readily tuned between ~5 nm to a few hundred nanometers through polymer solution concentration, viscosity, and electrospinning conditions such as nozzle-substrate bias.[24] In this study, we choose PVP as a model system for two reasons. First, we found that the interaction between phenol side groups and metal cations helps to promote the growth of smooth and continuous GNRs (see Supporting Information, Figure S6). Second, the benzene moieties in the polymer may act as nucleation cites for the graphitization of carbon sources and facilitate the formation of highly crystalline GNRs. The formation of electrospun PVP fibers has been reported previously.[24] We choose Pd as the catalyst for its high catalytic activity for graphitization reactions as well as its high melting point,[25] which further prevents surface migration of the catalyst. Figure 1 illustrates the schematic of our polymer-templated GNR synthesis. Briefly, PVP and palladium acetate [$Pd(OAc)_2$] were first dissolved in THF to concentrations of 30% w/v and 4.5–45 mg/mL respectively. Surfactants (e.g., MiTMAB) were added to tune the viscosity of the solution. Pd@PVP nanofibers were then electrospun onto the growth substrate (sapphire, quartz or Si/SiO_2) to form a random network (Figure 1a). Alternatively, the nanofibers can be collected on a metallic rotor with a gap that serves to align the nanofibers,[26] and then transferred onto the growth substrate (Figure 1b). The wafers containing electrospun polymers were subsequently placed in a furnace and subjected to high-temperature CVD treatments (see Supporting Information). GNRs can be grown over a large scale, which is only restricted by the equipment (Figure 1c).

Morphology Characterizations of GNRs. We first use scanning electron microscopy (SEM) to obtain a comprehensive view of the surface morphology before and after growth. The SEM micrographs (Figure 2a,b) reveal several interesting features. First, the postgrowth substrate (Figure 2b) shows a random network of 1D structures, which resembles the morphology of the polymer fibers before growth (Figure 2a). Second, the 1D structures on the postgrowth substrates are extremely long, easily spanning the size of the entire growth wafer. The length is dependent on the size of the substrate. This is in clear contrast to the much shorter GNRs obtained from Ni nanobar or DNA templates.[20,21] Finally, the widths of the 1D structures are uniform along their axial direction. At the crossing points (arrow, Figure 2b), the 1D structures are fused together and show locally larger width than the rest of the ribbons. This is likely due to locally excessive incorporation of the carbon source. Notably, the electrospun polymer fibers can be aligned on the substrate,[26] providing additional control over the polymer template morphology. To demonstrate this, we electrospun nanofibers onto a metallic rotor with a 3 mm gap and then transferred the aligned nanofibers inside the gap onto the growth substrate (Figure 1b).[26] As shown in Figure 2c, the Pd@PVP fibers are indeed uniaxially aligned. After high-temperature CVD, the parallel line structures are preserved (Figure 2d), suggesting that these postgrowth 1D structures are templated by the polymer nanofibers. The uniaxial alignment is further confirmed by the fast Fourier transform (FFT) patterns of the corresponding SEM images (insets, Figure 2c,d). The aligned nanofibers and postgrowth nanoribbons show highly anisotropic FFT patterns with narrow angular distribution of the intensities. On the other hand, the random network of nanofibers gives more isotropic FFT pattern (Figure S1). This indicates that by controlling the electrospinning condition, we are able to modify the orientation distribution of the fibers as well as the postgrowth nanoribbons.

The key hypothesis in our polymer-templated GNR synthesis approach is that the width of the polymer templates defines the width of the resultant nanoribbons. To test this hypothesis, we engineered both the electrospinning and CVD processes to control the widths of the as-spun polymer fibers and the

dx.doi.org/10.1021/ja509871n | J. Am. Chem. Soc. 2014, 136, 17284–17291

postgrowth nanoribbons. Smaller width is desired for GNRs in order to enhance bandgap and enable room-temperature FET operation. We discovered that the addition of surfactants, the Pd^{2+} concentration, the temperature ramping rate and the CH_4:H_2 ratio during CVD can all drastically affect the morphology of the postgrowth nanoribbons (see Supporting Information, Figure S4−5). Figure 2e and f show the AFM images of pre- and postgrowth nanoribbons at typical condition (45 mg/mL $Pd(OAc)_2$, see Supporting Information for other parameters). Most notably, both the width and height of the postgrowth nanoribbons are significantly smaller than those of the polymer nanofiber templates (Figure 2g−j): the width and height were reduced by 40 and 90%, respectively. This shrinkage is likely due to vaporization and/or graphitization of the polymer template at elevated temperatures. Moreover, the isotropic cross section of the polymer templates (width:height = 1.2) became highly anisotropic (width:height =7.8) after CVD. The resultant nanoribbons have an average height and width of 11 and 81 nm, respectively; these dimensions fall in the range of few-layer GNRs. Extremely narrow nanoribbons with 10 nm width and over 3.5-μm length can be observed (Figure 2f). On the other hand, we also note that some of the resultant nanoribbons are substantially thicker and should be termed graphitic nanoribbons (GraNRs). Further optimization of the synthetic parameters can be made to reduce the width/height of the postgrowth ribbons as well as their distributions. Nevertheless, these observations clearly indicate that the critical dimensions of the postgrowth nanoribbons are confined by those of the polymer templates, and extremely thin nanoribbons can be synthesized by further shrinkage of the width/height of the templates during the CVD process.

Structure Characterizations of GNRs. Subsequently, we gain insight of the structure of the postgrowth nanoribbons using microscopic Raman spectroscopy. Figure 3a shows a postgrowth nanoribbon with metal electrodes laid down for further electrical characterizations (see below). The width and height of this nanoribbon are 54 and 2 nm, respectively. Raman spectrum taken at the center of this nanoribbon (Figure 3a) shows strong D- and G-bands that are characteristic of narrow GNRs, as well as an obvious 2D band (Figure 3b). The full width at half-maximum (fwhm) of the G peak is 79.1 cm^{-1}, which is much smaller than that of amorphous carbon,[27] indicating a high graphitization degree in the postgrowth nanoribbons. The intensity ratio between D- and G-bands is 0.95, comparable to or smaller than that in GNRs from unzipping CNTs.[14,28,29] In literature the D band is usually attributed to the edge states of GNRs.[14,29] The existence of the 2D band further confirms that our postgrowth nanoribbons are highly graphitized. The broadening of the 2D peak can be attributed to the large portion of edge atoms or the relatively small graphitic domain sizes.[30,31] We note that the G and 2D bands of our polymer-derived GNRs are broader than those of unzipped CNTs or lithographically defined GNRs.[14,29] This broadening is attributed to the relatively small graphitic domain size, as will be discussed below. Intensity mappings of the D, G and 2D bands agree well with the morphology of the nanoribbon on the surface (Figure 3c−e). Taken together, these evidence confirm that our high-temperature CVD process on electrospun polymer templates yields GNRs with a high degree of graphitization.

To further characterize the degree of graphitization of the GNRs, as well as to directly observe the graphene domain, we carried out high-resolution TEM experiments (see Supporting Information). Figure 4a shows an overview of a representative

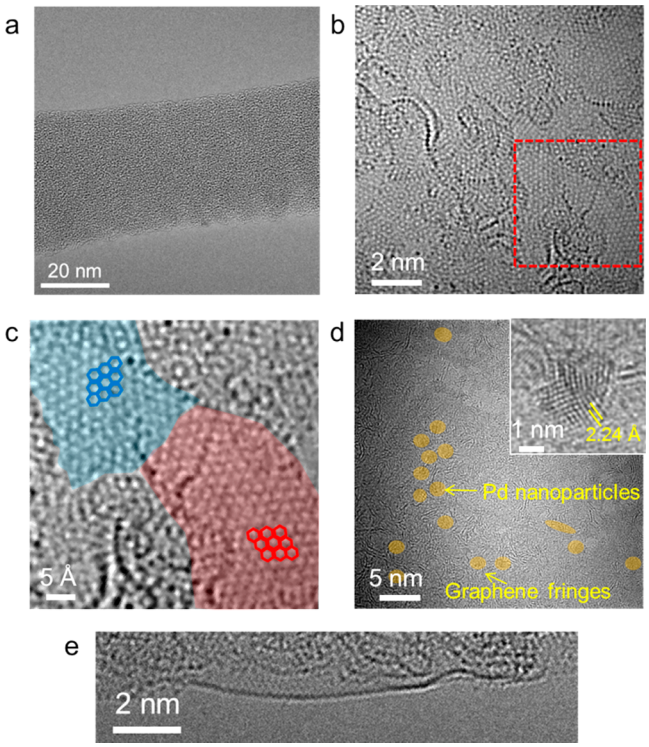

Figure 4. Atomic-resolution TEM images of GNRs grown from electrospun Pd@PVP. (a) An overview of a representative GNR. (b) Large-area view of a GNR. (c) Zoom-in view of the region marked by dotted red square in (b). Two graphitic domains are rendered red and blue, respectively. The red and blue solid lines are eye guides highlighting the hexagonal lattices. (d) Large-area view of a GNR region with Pd nanoparticles. Inset, zoom-in view of the Pd nanoparticle. (e) Edge structure of a GNR.

GNR which clearly exhibits a ribbon-like morphology. The width of this ribbon is about 40 nm. Figure 4b is an atomic-resolution image of the GNR templated by electrospun PVP. Multiple crystalline domains are evidently visible suggesting the polycrystalline nature of our GNRs. Further zoom-in view (Figure 4c) shows that each single-crystalline domain (red and blue regions, Figure 4c) has a hexagonal lattice with lattice spacing (2.46 Å) corresponding to that of graphene. The size of polycrystalline domain falls in the range of 2−20 nm as determined from tens of TEM images. Another application of this technique is to image the interface between metal catalyst and graphitic structures in GNRs, which shed light on the catalytic mechanism of graphitization. As shown in Figure 4d, embedded nanoparticles with average size of 1 nm (yellow circles, Figure 4d) can be distinguished by contrast from the carbon matrix. Zoom-in view of an individual nanoparticle (inset, Figure 4d) shows that it is highly crystalline with lattice spacing of 2.24 Å that matches the [111] lattice spacing of face-centered-cubic (fcc) Pd. The $Pd(OAc)_2$ in the pregrowth polymer nanofibers are reduced to Pd likely during the CVD process. The graphene domains tightly surround the Pd nanoparticles, suggesting that the Pd catalyzes the graphitization. The fringe spacing in the graphitic regions is ~0.35 nm, closely matching the interplane spacing of graphene. Moreover, the GNRs show quite smooth edge as shown in Figure 4e. To

dx.doi.org/10.1021/ja509871n | J. Am. Chem. Soc. 2014, 136, 17284−17291

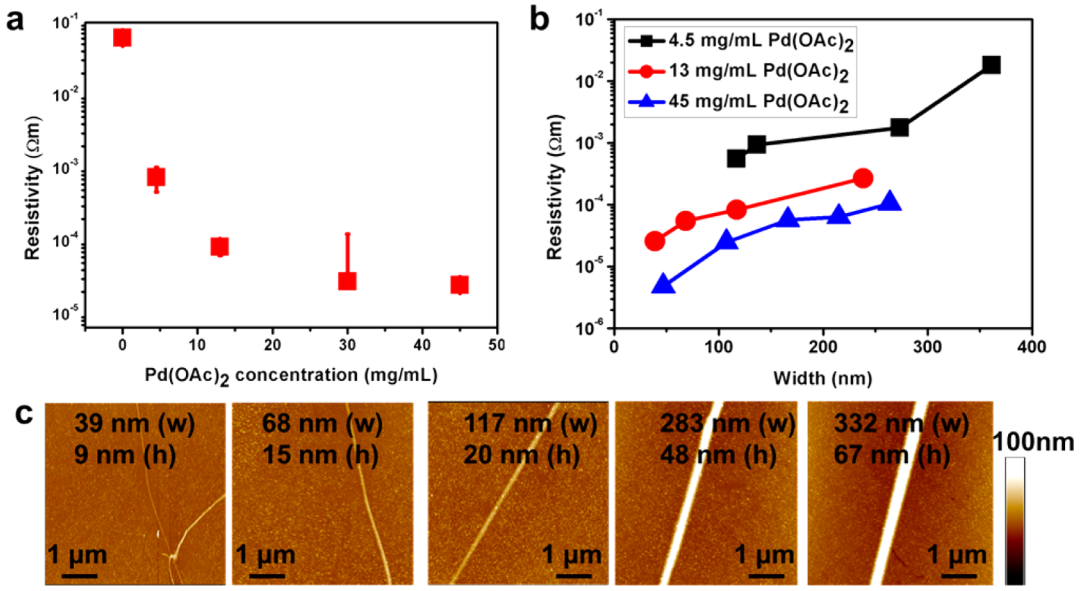

Figure 5. Resistivity of single GNRs templated by electrospun-PVP. (a) Resistivity of GNRs as a function of $Pd(OAc)_2$ concentration. The width of the nanoribbons for 0, 4.5, 13, 30 and 45-mg/mL Pd catalyst are ~3 μm, ~117 nm, ~117 nm, ~130 nm, and ~107 nm, respectively. (b) Resistivity of GNRs as a function of the width of GNR at given $Pd(OAc)_2$ concentrations (black rectangular: 4.5 mg/mL; red circles: 13 mg/mL; blue triangles: 45 mg/mL). (c) AFM images of GNRs with different widths synthesized from PVP templates loaded with 13 mg/mL $Pd(OAc)_2$.

understand the catalytic effect of Pd, we synthesized nanoribbons from the PVP templates without Pd using identical CVD conditions. Very different from those synthesized with the Pd catalyst, the postgrowth ribbons are even wider than the original electrospun PVP (see Supporting Information, Figure S8). Drastically, only a small portion of the Pd-free GNRs could be stably imaged under TEM while the majority of them disintegrate immediately upon electron-beam irradiation. We further compare the average grain size of the stable (presumably more graphitic) portion of the Pd-free GNRs to those with 9 mg/mL Pd loading by using the Scherrer equation on the FFT patterns of their corresponding TEM images (see Supporting Information, Figure S13). The 50% increase of the domain size by the addition of a small amount of Pd further confirms the critical role of Pd catalysis in the growth of highly graphitized GNRs.

Electronic Properties of GNRs. To evaluate the conductivity of the electrospun PVP-templated GNRs, we performed four-probe resistance measurement on single GNRs (see Supporting Information, Figure S3). First, we compare the resistivity (in Ωm) of GNRs with similar widths (~120 nm) prepared at different Pd^{2+} concentrations (Figure 5a). We note that without the Pd catalyst, the resultant ribbons are substantially wider, and the smallest resistivity measured from a 3-μm-wide ribbon was plotted. Most noticeably, the resistivity of the postgrowth GNRs dropped by almost 2 orders of magnitude by addition of a small amount (4.5 mg/mL) $Pd(OAc)_2$ to the polymer template. This decreased resistivity is attributed to the higher degree of graphitization. Indeed, XPS on the C 1s state reveals a higher sp^2- to sp^3-carbon ratio in the GNR samples synthesized with higher Pd concentration (see Supporting Information, Figure S11). The resistivity of the 120 nm-wide GNRs saturates at $>10^{-5}$ Ωm with Pd concentrations beyond 30 mg/mL. This saturation combined with the XPS data clearly indicates that the decreased resistivity is due to higher degree of graphitization rather than higher Pd concentration in the resultant GNRs. The Pd nanoparticles are highly discontinuous and should not dominate the transport behavior of the GNRs. Furthermore, these Pd catalysts can be removed by chemical etching after the growth (see Supporting Information, Figure S12).

In addition to the loading of metal ions, we investigated the correlation between the dimension of GNRs and the resistivity. Figure 5b shows the resistivity of GNRs as a function of width at given Pd concentrations (4.5, 13, and 45 mg/mL). It should be noted that the thicknesses of the GNRs increase with their widths (Figure 5c). Some of the nanoribbons have thicknesses more than a few layer of graphene, and should be categorized as graphitic nanoribbons (GraNRs) instead. Interestingly, we find that for the three concentrations, the resistivity shows a monotonic decrease as the width of the GNRs shrinks from 350 to 50 nm. This is in drastic contrast to the resistivity of GNRs etched from graphene sheets, where narrower widths lead to larger resistivity due to higher density of defects.[32] The reversed trend in our case is possibly due to lower density of nucleation sites of graphitic domains, as less Pd is present in the polymer fiber. This likely leads to lower density of domain boundaries and higher degree of graphitization. The lowest resistivity, 4.8×10^{-6} Ωm, was observed in 50 nm-wide GNRs synthesized with 45 mg/mL Pd catalyst. This resistivity is comparable with that of the bulk graphite and GNRs derived from etching methods,[14,22] and about 3 orders of magnitude lower than that of the carbon fibers from pyrolysis.[33] Further investigation of structural difference in our polymer-templated GNRs of different widths will yield more insight of the mechanism; however, the lower resistivity of narrower GNRs holds great promise to create highly conductive GNRs with ultrasmall dimensions by our approach.

The lateral confinement of graphene within a 1D form as well as edge- and body-scattering centers can open up a transport bandgap in GNRs, allowing them to function as FETs.[34] To this end, we fabricated bottom-gated GNR-FETs from narrow, highly graphitized GNRs. Briefly, the as-synthesized GNRs were transferred onto a highly doped Si

dx.doi.org/10.1021/ja509871n | J. Am. Chem. Soc. 2014, 136, 17284−17291

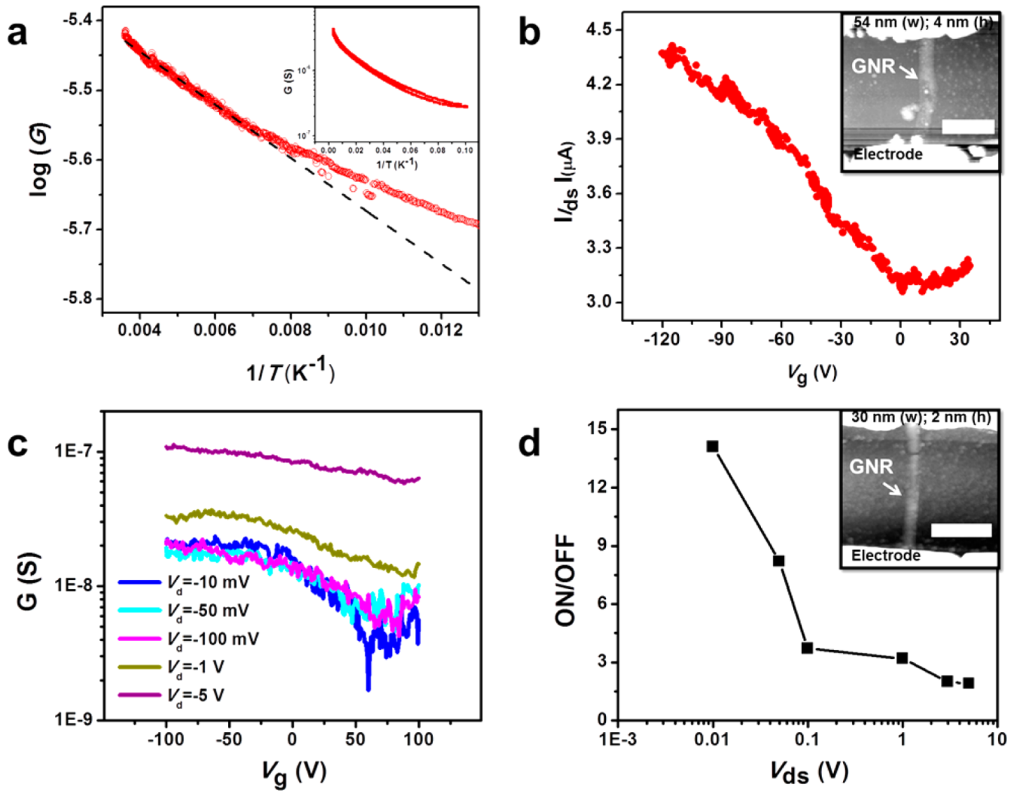

Figure 6. Electrical transport properties of GNRs. (a) Semilogarithmic G vs $1/T$ plot of a GNR with 54 nm width and 4 nm height, measured by four-probe method at a constant current bias of 1 μA. (b) I_{ds} vs V_g plot measured from the same device in (a) (V_{ds} = −0.1 V). The inset shows the AFM image of the device (only two contacts are shown. The scale bar is 500 nm). (c) Conductance vs V_g plots of a 30 nm-wide GNR-FET scanned at different V_{ds}. (d) The on/off ratio as a function of V_{ds} for the device in (c). The inset shows the AFM image of the device and the scale bar is 500 nm. Data in (b−d) were taken at ambient condition.

substrate with 300 nm SiO_2 on top. Source and drain electrodes (Ti/Pd) were defined by standard electron-beam lithography and metallization. The Si back plane and the SiO_2 layers are used as the back-gate electrode and gate dielectric, respectively. We first performed temperature-dependent four-probe resistivity characterization on a GNR with 54 nm width and 4 nm height (Figure 6a,b inset). The Si back-gate was grounded for this measurement, which set the conductance of this particular device at minimum (Figure 6b). The monotonic decrease of conductance (G) as a function of $1/T$ in the temperature range of 300 to 10 K (inset, Figure 6a) indicates the semiconducting nature of the GNR.[35] Notably, there is no hysteresis in the G vs $1/T$ curves when the sample is cycled between 10 and 300 K, suggesting the absence of mobile charges on the surface.[36] Moreover, the linear regime of the semilogarithmic G vs $1/T$ curve in the range of 278−100 K can be fitted to an Arrhenius equation, i.e., $G = \exp(((-E_a)/(2k_BT)))$, where k_B is the Boltzmann constant and the E_a is the activation energy. The fitting suggests that the transport is dominated by thermally activated charge carriers in this temperature range. Fitting of the data yields an E_a of 15.0 meV, which roughly corresponds to the transport gap in this range.[34] The G vs $1/T$ curve deviates from the Arrhenius plot in the temperature range below 100 K, suggesting a different transport mechanism such as variable range hopping.[20,34]

Next, we tested the drain-source current (I_{ds}) as a function of back-gate voltage (V_g) at ambient conditions on the same device. The GNR-FET shows ambipolar transport characteristics with charge neutrality point at 0 V (Figure 6b). The field-effect mobility extracted from the linear regime of the I_{ds}−V_g curve is 28 $cm^2/(V\ s)$ (see Supporting Information), comparable to that of GNRs grown from metallic nanotemplates and substantially larger than obtained from DNA-templated GNRs.[20,21] A larger gate modulation can be achieved from a narrower, 30 nm GNR-FET (Figure 6d inset). We measured the I_{ds} vs V_g curves on this device at different V_{ds} biases (Figure 6c). It can be seen that the on/off ratio of the devices significantly increases with decreased V_{ds} (Figure 6d). The strong dependence of on/off ratio on V_{ds} suggests that edge scattering centers and Coulomb blockade effect of the graphitic domains of our GNRs may contribute to the transport gap in addition to the lateral quantum confinement.[20,34] A room-temperature on/off ratio of ∼14 can be achieved with V_{ds} of −10 mV, comparable to that from GNRs grown on Ni nanobars.[20] Further improvement of the device performance can be achieved by, for example, using a high-dielectric-constant gate.

We note that our polymer-templated GNRs consist of a multitude of graphitic domains, which leads to transport behavior different from unzipped CNTs or lithography-defined GNRs that have continuous hexagonal lattices. On one hand, the transport gap observed in our GNR device cannot be compared directly with those obtained experimentally and theoretically for single-crystalline monolayer GNRs,[10,37] as defects in our structures can contribute to the transport gap along with lateral quantum confinement.[34] On the other hand, the grain boundaries serve as scattering centers that limit the mobility in our GNR-FETs. Further improvement can be made to increase the domain size polymer templates selection and

dx.doi.org/10.1021/ja509871n | J. Am. Chem. Soc. 2014, 136, 17284−17291

further optimization of the growth conditions such as catalyst type and concentration, growth atmosphere and temperature.

CONCLUSIONS

In summary, we developed a scalable method to fabricate GNRs from electrospun polymer templates. Highly crystalline GNRs with tunable width down to ~10 nm and resistivity as low as 4.8×10^{-6} Ωm can be achieved by Pd-catalyzed CVD using 1D PVP nanofibers as the growth template. The narrow GNRs can function as FETs at room temperature. Compared to GNRs derived from DNA templates,[21] our results show more than 2 orders of magnitude improvement in terms of conductivity and mobility, as well as much higher scalability. Moreover, the generality of this method will allow us to explore a large variety of polymer templates and investigate the effect of their compositions and structures on the dimension and electrical characteristics of the GNRs. Coupled with the high scalability and low cost of the electrospinning technique, this approach has great potential for mass production of high-quality GNRs for a wide range of applications in flexible digital electronics, electronic skins and sensor devices.

ASSOCIATED CONTENT

Supporting Information

Experimental details. Additional SEM, TEM, XPS, EDS and EELS data. Analysis of graphitic domain sizes. This material is available free of charge via the Internet at http://pubs.acs.org.

AUTHOR INFORMATION

Corresponding Author

zbao@stanford.edu

Present Address

[▽]The Dow Chemical Company, Midland, Michigan 48674, United States.

Notes

The authors declare no competing financial interest.

ACKNOWLEDGMENTS

We are grateful to the Global Climate and Energy Project (GCEP) for the support of this work. Dr. H. T. Yuan, Prof. Y. Cui and Prof. H. Y. Hwang are supported by the Department of Energy, Office of Basic Energy Sciences, Division of Materials Sciences and Engineering, under contract DE-AC02-76SF00515. We thank Dr. C. J. Shih for helpful discussion.

REFERENCES

(1) Novoselov, K. S.; Geim, A. K.; Morozov, S. V.; Jiang, D.; Zhang, Y.; Dubonos, S. V.; Grigorieva, I. V.; Firsov, A. A. *Science* **2004**, *306*, 666−669.

(2) Novoselov, K.; Geim, A. K.; Morozov, S.; Jiang, D.; Katsnelson, M.; Grigorieva, I.; Dubonos, S.; Firsov, A. *Nature* **2005**, *438*, 197−200.

(3) Lin, Y.-M.; Dimitrakopoulos, C.; Jenkins, K. A.; Farmer, D. B.; Chiu, H.-Y.; Grill, A.; Avouris, P. *Science* **2010**, *327*, 662.

(4) Bae, S.; Kim, H.; Lee, Y.; Xu, X.; Park, J.-S.; Zheng, Y.; Balakrishnan, J.; Lei, T.; Kim, H. R.; Song, Y. I. *Nat. Nanotechnol.* **2010**, *5*, 574−578.

(5) Han, T.-H.; Lee, Y.; Choi, M.-R.; Woo, S.-H.; Bae, S.-H.; Hong, B. H.; Ahn, J.-H.; Lee, T.-W. *Nat. Photonics* **2012**, *6*, 105−110.

(6) Xia, F.; Mueller, T.; Lin, Y.-m.; Valdes-Garcia, A.; Avouris, P. *Nat. Nanotechnol.* **2009**, *4*, 839−843.

(7) Zhu, Y.; Murali, S.; Stoller, M. D.; Ganesh, K. J.; Cai, W.; Ferreira, P. J.; Pirkle, A.; Wallace, R. M.; Cychosz, K. A.; Thommes, M.; Su, D.; Stach, E. A.; Ruoff, R. S. *Science* **2011**, *332*, 1537−1541.

(8) Yoo, E.; Kim, J.; Hosono, E.; Zhou, H.-s.; Kudo, T.; Honma, I. *Nano Lett.* **2008**, *8*, 2277−2282.

(9) Geim, A. K.; Novoselov, K. S. *Nat. Mater.* **2007**, *6*, 183−191.

(10) Li, X.; Wang, X.; Zhang, L.; Lee, S.; Dai, H. *Science* **2008**, *319*, 1229−1232.

(11) Bai, J.; Zhong, X.; Jiang, S.; Huang, Y.; Duan, X. *Nat. Nanotechnol.* **2010**, *5*, 190−194.

(12) Tapaszto, L.; Dobrik, G.; Lambin, P.; Biro, L. P. *Nat. Nanotechnol.* **2008**, *3*, 392−401.

(13) Jiao, L.; Zhang, L.; Wang, X.; Diankov, G.; Dai, H. *Nature* **2009**, *458*, 877−880.

(14) Jiao, L.; Wang, X.; Diankov, G.; Wang, H.; Dai, H. *Nat. Nanotechnol.* **2010**, *5*, 321−325.

(15) Wang, X.; Ouyang, Y.; Jiao, L.; Wang, H.; Xie, L.; Wu, J.; Guo, J.; Dai, H. *Nat. Nanotechnol.* **2011**, *6*, 563−567.

(16) Sprinkle, M.; Ruan, M.; Hu, Y.; Hankinson, J.; Rubio-Roy, M.; Zhang, B.; Wu, X.; Berger, C.; Heer, W. A. D. *Nat. Nanotechnol.* **2010**, *5*, 727−731.

(17) Fan, S.; Chapline, M. G.; Franklin, N. R.; Tombler, T. W.; Cassell, A. M.; Dai, H. *Science* **1999**, *283*, 512−514.

(18) Li, X.; Cai, W.; An, J.; Kim, S.; Nah, J.; Yang, D.; Piner, R.; Velamakanni, A.; Jung, I.; Tutuc, E. *Science* **2009**, *324*, 1312−1314.

(19) Martin-Fernandez, I.; Wang, D.; Zhang, Y. *Nano Lett.* **2012**, *12*, 6175−6179.

(20) Kato, T.; Hatakeyama, R. *Nat. Nanotechnol.* **2012**, *7*, 651−656.

(21) Sokolov, A. N.; Yap, F. L.; Liu, N.; Kim, K.; Ci, L.; Johnson, O. B.; Wang, H.; Vosgueritchian, M.; Koh, A. L.; Chen, J. *Nat. Commun.* **2013**, *4*, No. 2402.

(22) Moore, A. *Chem. Phys. Carbon* **1973**, *11*, 69.

(23) Huang, Z.-M.; Zhang, Y. Z.; Kotaki, M.; Ramakrishna, S. *Compos. Sci. Technol.* **2003**, *63*, 2223−2253.

(24) Kenawy, E.-R.; Abdel-Fattah, Y. R. *Macromol. Biosci.* **2002**, *2*, 261−266.

(25) Scheuermann, G. M.; Rumi, L.; Steurer, P.; Bannwarth, W.; Mulhaupt, R. *J. Am. Chem. Soc.* **2009**, *131*, 8262−8270.

(26) Li, D.; Xia, Y. *Adv. Mater.* **2004**, *16*, 1151−1170.

(27) Freire, F., Jr; Achete, C.; Mariotto, G.; Canteri, R. *J. Vac. Sci. Technol., A* **1994**, *12*, 3048−3053.

(28) Zhang, Z.; Sun, Z.; Yao, J.; Kosynkin, D. V.; Tour, J. M. *J. Am. Chem. Soc.* **2009**, *131*, 13460−13463.

(29) Ryu, S.; Maultzsch, J.; Han, M. Y.; Kim, P.; Brus, L. E. *ACS Nano* **2011**, *5*, 4123−4130.

(30) Ferrari, A. C. *Solid State Commun.* **2007**, *143*, 47−57.

(31) Malard, L. M.; Pimenta, M. A.; Dresselhaus, G.; Dresselhaus, M. S. *Phys. Rep.* **2009**, *473*, 51−87.

(32) Bai, J.; Duan, X.; Huang, Y. *Nano Lett.* **2009**, *9*, 2083−2087.

(33) Inagaki, M.; Yang, Y.; Kang, F. *Adv. Mater.* **2012**, *24*, 2547−2566.

(34) Han, M. Y.; Brant, J. C.; Kim, P. *Phys. Rev. Lett.* **2010**, *104*, 056801.

(35) Ashcroft, N. W. M. N. D. *Solid State Physics*, 1976, 563−565.

(36) Skakalova, V.; Kaiser, A. B.; Yoo, J. S.; Obergfell, D.; Roth, S. *Phys. Rev. B: Condens. Matter Mater. Phys.* **2009**, *80*, 153404.

(37) Son, Y.-W.; Cohen, M. L.; Louie, S. G. *Phys. Rev. Lett.* **2006**, *97*, 216803.